Stable, free-standing Ge nanocrystals

I.D. Sharp,[a,b] Q. Xu,[a,b] C.Y. Liao,[a,b] D.O. Yi,[a,c] J.W. Beeman,[a] Z. Liliental-Weber,[a] K.M. Yu,[a] D.N. Zakharov,[a] J.W. Ager III,[a] D.C. Chrzan,[a,b] and E.E. Haller[a,b]

[a] Materials Sciences Division, Lawrence Berkeley National Laboratory, Berkeley, CA 94720
[b] Department of Materials Science and Engineering, University of California, Berkeley, CA 94720
[c] Applied Science and Technology, University of California, Berkeley, CA 94720

ABSTRACT

Free-standing Ge nanocrystals that are stable under ambient conditions have been synthesized in a two-step process. First, nanocrystals with a mean diameter of 5 nm are grown in amorphous SiO_2 by ion implantation followed by thermal annealing. The oxide matrix is then removed by selective etching in diluted HF to obtain free-standing nanocrystals on a Si wafer. After etching, nanocrystals are retained on the surface and the size distribution is not significantly altered. Free-standing nanocrystals are stable under ambient atmospheric conditions, suggesting formation of a self-limiting native oxide layer. For free-standing as opposed to embedded Ge nanocrystals, an additional amorphous-like contribution to the Raman spectrum is observed and is assigned to surface reconstruction-induced disordering of near-surface atoms.

PACS numbers: 81.07.-b; 63.22.+m; 68.35.Ja; 68.47.Fg

Ge nanocrystals have attracted considerable attention because of their potential applications in non-volatile memory and integrated optoelectronics, as well as the prospect for discovering new physical phenomena. A number of groups have reported synthesis of Ge nanocrystals in amorphous SiO_2 matrices.[1] Embedded nanocrystals are useful for solid-state device fabrication and testing, but the presence of a surrounding matrix precludes the use of many surface-sensitive characterization methods. Therefore, it is desirable to develop a method to selectively remove the matrix to enable surface characterization, direct contact measurement, and comparative studies of embedded and free-standing nanocrystals. We report here such a method and use it to compare the vibrational properties of embedded and free-standing Ge nanocrystals.

Ion implantation of ^{70}Ge was performed at 50 keV ($1x10^{16}$ cm^{-2}), 80 keV ($1.2x10^{16}$ cm^{-2}), and 120 keV ($2x10^{16}$ cm^{-2}) into 500 nm thick wet oxide layers grown on (100) Si. Nanocrystals were subsequently grown by thermal annealing in an Ar atmosphere at 900 °C for one hour, followed by quenching. The 500 nm thick SiO_2 matrix was selectively removed by etching in 1:1 49% HF:H_2O.[2] Samples were immersed in methanol to terminate etching and were dried under flowing N_2. A similar HF etching procedure was recently employed to study the photoluminescence behavior of free standing Si nanocrystals.[3]

Transmission electron micrographs of embedded nanocrystal samples demonstrate that nanocrystals are spherical with an average size of 5.1 nm and a distribution full width at half maximum (FWHM) of 3.9 nm [Fig. 1(a)]. Electron diffraction patterns obtained after etching show that Ge nanoparticles remain crystalline.

Some etched samples were placed in methanol and sonicated in order to reduce

the nanocrystal surface density to a few hundred per 4 μm^2 scan window and allow for atomic force microscopy of isolated nanocrystals. Out of plane (height) AFM data were used to measure the overall nanocrystal size distribution. The mean nanocrystal size after etching, as determined by AFM, is 5.1 nm with a distribution FWHM of 3.4 nm [Fig. 1(b)],[4] in excellent agreement with results obtained via TEM [Fig. 1(a)]. Consequently, this process may be used to rapidly determine nanocrystal size distributions and to directly compare the properties of embedded and free-standing Ge nanocrystals.

Figure 2(a) shows a Ge 3d x-ray photoelectron spectroscopy (XPS) spectrum obtained after exposure of free-standing nanocrystals to ambient conditions for 2 h. A strong peak originating from Ge-Ge bonding is observed at 29.4 eV along with a slight shoulder at higher binding energies indicative of a small amount of a Ge suboxide. As shown in Fig. 2(b), after extended exposure of free-standing nanocrystals to ambient conditions a peak associated with GeO_x ($x \approx 2$) emerges near 32.4 eV.

In semiconductor nanocrystals, confinement of optical phonons leads to relaxation of the $\vec{q} \cong 0$ selection rules for Raman scattering. As a result, optical phonons with $\vec{q} \neq 0$ are excited and Raman spectra from nanocrystal samples should be asymmetrically broadened and redshifted relative to bulk spectra.[5,6] Figure 3(a) shows a spectrum from an as-grown ^{70}Ge nanocrystal sample, after subtraction of the second order features from the Si substrate. As expected, the Raman line is asymmetrically broadened. However, the line position is blue shifted with respect to the line of an isotopically enriched bulk crystal [Fig. 3(e)]. We have shown previously that the observed blueshift is due to matrix-induced compressive stress and can be controllably relaxed via post-growth thermal annealing.[7]

As shown in Fig. 3(b), immediately after etching the Ge nanocrystal Raman line position is redshifted with respect to that of the bulk reference, in good agreement with theoretical predictions.[5,6] Furthermore, Raman spectra (shape and position) of etched samples are not affected by etching times ranging from 1 min to 1 hour, confirming that the nanocrystals are stable in the HF etchant. We conclude from these Raman data that the primary effect of etching is to remove the matrix-induced compressive stress and that the nanocrystal size distribution is not significantly changed. This is consistent with the AFM data discussed above.

A prominent feature of Raman spectra of exposed nanocrystals is the enhanced scattering intensity below 275 cm^{-1}. This can be seen in Fig. 3(c), which was obtained by subtracting the spectrum in Fig. 3(a) from the spectrum in Fig. 3(b) after shifting the as-grown spectrum along the x-axis to compensate for the compressive stress. The resulting difference spectrum resembles that of amorphous ^{nat}Ge [Fig. 3(d)]. However, HF etching is not expected to amorphize nanocrystals and electron diffraction patterns confirm that the exposed clusters remain crystalline. Thus, we consider the effect of surface reconstruction-induced disordering on Raman scattering.

Direct evidence of disordered shells surrounding free-standing Ge nanocrystals, without exposure to air, was recently demonstrated by Williamson *et al*.[8] who compared the results of photoemission measurements to first principles structure calculations. They showed that the observed valence band density of states can be explained by a distorted diamond structure arising from surface reconstruction-induced bond length and angle distribution broadening. A similar photoemission study, on somewhat larger nanocrystals, showed that the Ge 3d spin-orbit splitting is consistent with a tetrahedrally-

coordinated core surrounded by a disordered shell that gives rise to amorphous-like broadening of the core-level shifts.[9] Furthermore, amorphous-like Raman scattering was observed previously from free-standing Ge, Si, and GaP nanocrystals formed by gas evaporation and was attributed to a disordered shell surrounding the crystalline core.[10] However, similar Raman spectra were not observed for embedded nanocrystals investigated by the same authors.[6,11] This difference was ascribed to free versus fixed boundary conditions for the vibrational amplitudes of the near-surface atoms. The presence of the matrix stabilizes the surface atoms and reduces their contribution to the Raman intensity, which is related to the square of the vibrational amplitude.

This explanation for the suppression of the amorphous-like contribution to Raman scattering of embedded nanocrystals is consistent with the present observations. Nevertheless, we consider additional mechanisms for suppression of the amorphous scattering in embedded nanocrystals. The phonon density of states is large in the oxide matrix in the energy range of the amorphous-like scattering observed in the free-standing nanocrystals;[12] this may enhance the decay rate of near-surface vibrations. Lifetime broadening of the phonon modes originating near the surfaces could then suppress observation of amorphous-like scattering. Alternatively, embedded nanocrystals might be passivated by the surrounding matrix such that reconstruction-induced disorder is not significant. Additional studies on embedded nanocrystals in different matrices and on exposed nanocrystals with various surface passivating layers may clarify the reasons for the absence of an amorphous-like contribution to Raman scattering from embedded nanocrystals.

Fundamental surface vibrational modes predicted by dynamical matrix calculations are expected to be rather sharp.[13] In the present case, broad Raman scattering is observed and we therefore conclude that the amorphous-like contribution does not originate from the fundamental surface vibrational modes predicted in Ref. 14. Rather, we attribute the observed scattering to surface reconstruction-induced disorder, in agreement with the interpretation in Refs. 9, 10, & 11. Differences between the spectra in Fig. 3(c) and Fig. 3(d) may reflect differences in the phonon density of states between disordered shells surrounding nanocrystals and bulk amorphous Ge.

Raman spectra of free-standing nanocrystals were obtained both immediately after etching and after long-term exposure to air. Though XPS results indicate that some oxidation of the nanocrystals occurs after extended exposure, the line positions of Raman spectra are not affected by exposure time and amorphous-like scattering is observed for all exposure times. Therefore, neither hydrogen passivation after short exposure times nor oxidation after extended exposure are sufficient to inhibit surface reconstruction and accompanying disorder.

It is not possible to use the XPS data to provide a quantitative measure of the oxide thickness because of the wide nanocrystal size distribution, unknown packing on the surface, and the non-planar geometry. Together, these effects likely lead to a significant over-sampling of the atoms nearest to the surface compared to those of a planar sample. However, growth of a full-thickness bulk-like native Ge oxide layer[14] (2 - 4 nm) would consume a considerable fraction of the nanocrystals and significantly broaden and redshift Raman spectra. Since this effect is not observed and the Ge-Ge bonding peak measured by XPS retains significant intensity after extended exposure, we

find that the nanocrystals must develop an oxide shell around the crystalline Ge core with a thickness less than that of a planar native oxide and this shell stabilizes the nanocrystal from further oxidation. Self-limiting, size-dependent native oxide formation has been observed previously for the case of Si nanowires[15] and nanocrystals[16] and was attributed to enhanced activation energy for oxygen diffusion through the highly curved and strained oxide skin. A similar process is likely to occur in the present case. Additional experiments using TEM will be performed to determine the native oxide thickness and kinetics of its formation.

In conclusion, we have developed a process to obtain free-standing Ge nanocrystals without altering the size distribution. The exposed nanocrystals are stable under ambient atmospheric conditions after formation of a native oxide shell that is considerably thinner than the bulk native oxide. Raman spectra of exposed nanocrystals exhibit amorphous-like vibrational modes that are consistent with surface reconstruction-induced disordering.

ACKNOWLEDGEMENTS

I.D.S. acknowledges support from the Intel Corporation. D.O.Y. acknowledges support from the Luce Foundation Fellowships. D.C.C. and E.E.H. acknowledge support from the Miller Institute for Basic Research in Science. This work is supported in part by the Director, Office of Science, Office of Basic Energy Sciences, Division of Materials Science and Engineering, of the U.S. Department of Energy under contract No. DE-AC03-76SF00098 and in part by U.S. NSF Grant Nos. DMR-0405472 and EEC-0085569.

FIGURE CAPTIONS

Fig. 1: Size distribution histograms of nanocrystals grown at 900 ^{o}C for 1 hour obtained using TEM giving a mean size of 5.1 nm and a FWHM of 3.9 nm (a), and AFM giving a mean size of 5.1 nm and a FWHM of 3.4 nm (b).

Fig. 2: Ge 3d XPS spectra of exposed nanocrystals 2 hours after (a) and 7 weeks after (b) selective removal of the SiO_2 matrix. The lower energy peak (29.4 eV) corresponds to Ge-Ge bonding in the nanocrystals. The higher energy peak (32.5 eV) in (b) is assigned to GeO_x ($x \leq 2$).

Fig. 3: Raman spectra obtained using 488 nm excitation with 5 cm^{-1} resolution. (a) As-grown ^{70}Ge nanocrystals embedded in a SiO_2 matrix, (b) free-standing ^{70}Ge nanocrystals after 2 hours of exposure to air, (c) spectrum in (a) subtracted from spectrum in (b) after shifting (a) to lower frequency to compensate for matrix-induced compressive stress (see text), (d) sputtered amorphous ^{nat}Ge, and (e) an isotopically enriched ^{70}Ge bulk crystal. The vertical dashed line indicates the peak position of the bulk reference sample. The Raman line position of exposed nanocrystals does not change after extended exposure to air. The spectrum in (c) has been multiplied by 2 for clarity.

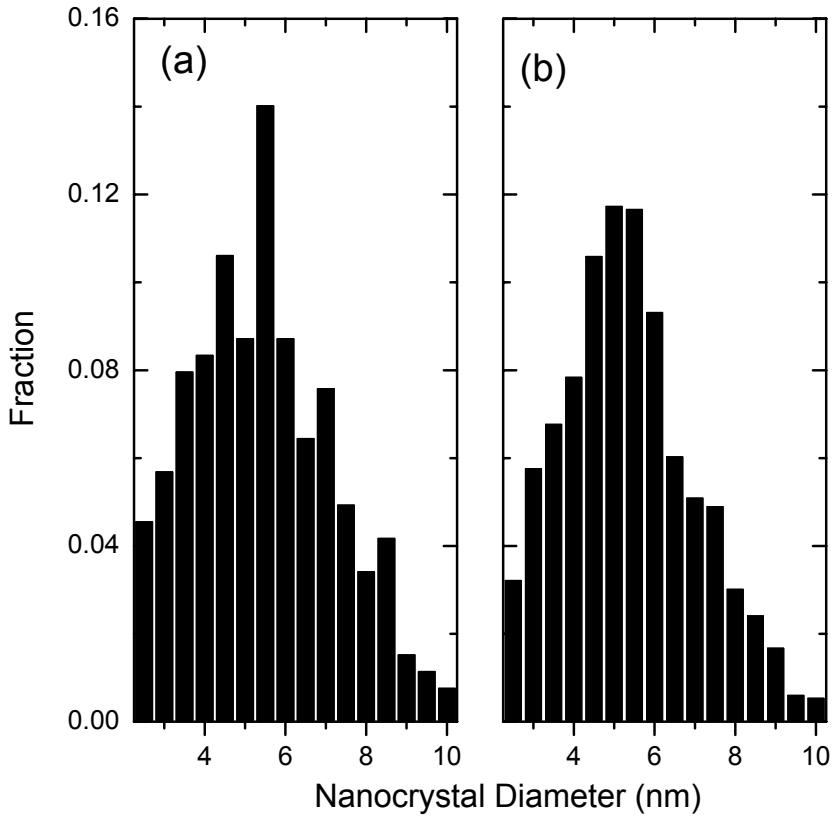
(a)
(b)
Fraction
0.16
0.12
0.08
0.04
0.00
4
6
8
10
Nanocrystal Diameter (nm)

Figure 1

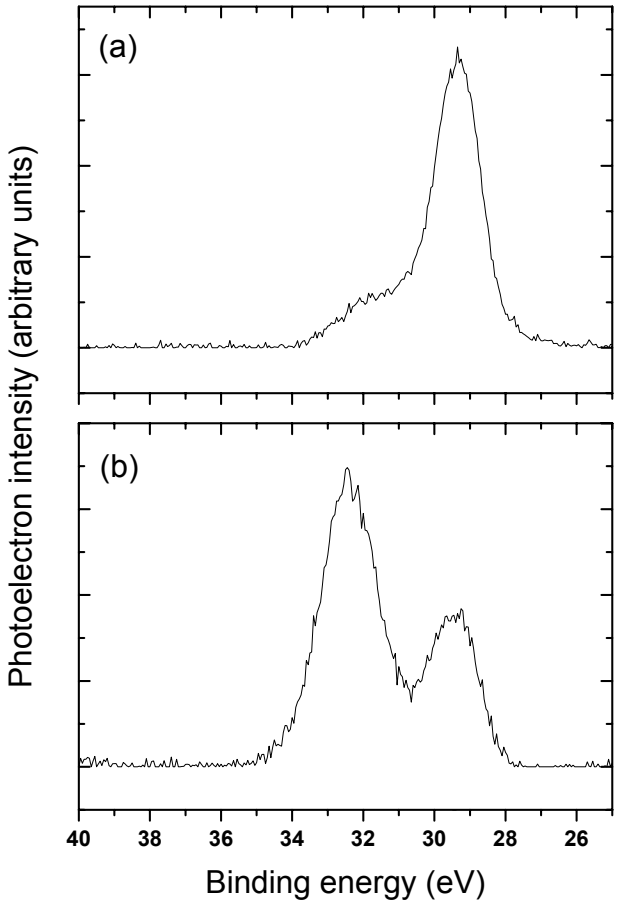
(a)
(b)
Photoelectron intensity (arbitrary units)
40
38
36
34
32
30
28
26
Binding energy (eV)

Figure 2

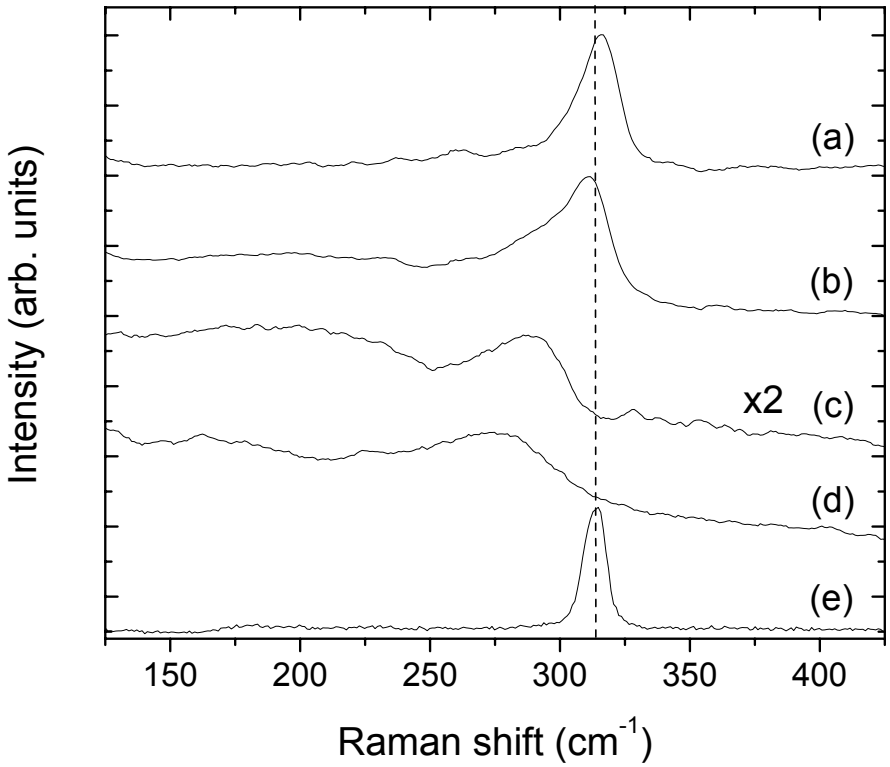
Intensity (arb. units)
(a)
(b)
x2
(c)
(d)
(e)
150
200
250
300
350
400
Raman shift (cm-1)

Figure 3

REFERENCES

1. A. Kanjilal, J. Lundsgaard Hansen, P. Gaiduk, A. Nylandsted Larsen, N. Cherkashin, A. Claverie, P. Normand, E. Kapelanakis, D. Skarlatos, and D. Tsoukalas, Appl. Phys. Lett. **82**, 1212 (2003); A. V. Kolobov, S. Q. Wei, W. S. Yan, H. Oyanagi, Y. Maeda, and K. Tanaka, Phys. Rev. B **67**, 195314 (2003); W.K. Choi, V. Ng, S.P. Ng, H.H. Thio, Z.X. Shen, and W.S. Li, J. Appl. Phys. **86**, 1398 (1999); M. Yamamoto, T. Koshikawa, T. Yasue, H. Harima, and K. Kajiyama, Thin Solid Films **369**, 100 (2000); W. Skorupa, L. Rebohle, and T. Gebel, Appl. Phys. A **76**, 1049 (2003).
2. I.D. Sharp, Q. Xu, C.Y. Liao, D.O. Yi, J.W. Ager III, J.W. Beeman, K.M. Yu, D.N. Zakharov, Z. Liliental-Weber, D.C. Chrzan, and E.E. Haller, Mat. Res. Soc. Symp. Proc. **818**, M13.3.1 (2004).
3. J.S. Biteen, N.S. Lewis, H.A. Atwater, and A. Polman, Appl. Phys. Lett. **84**, 5389 (2004).
4. To ensure the accuracy of these measurements, the AFM was calibrated with Au nanoparticles of well-known size distribution deposited on a bare Si substrate.
5. H. Richter, Z.P. Wang, and B. Ley, Solid State Commun. **39**, 625 (1981); I.H. Campbell and P.M. Fauchet, Solid State Commun. **58**, 739 (1986).
6. Minoru Fujii, Shinji Hayashi, and Keiichi Yamamoto, Jpn. J. Appl. Phys. **30**, 687 (1991).
7. I.D. Sharp, D.O. Yi, Q. Xu, C.Y. Liao, J.W. Ager III, J.W. Beeman, Z. Liliental-Weber, K.M. Yu, D. Zakharov, D.C. Chrzan, and E.E. Haller, Appl. Phys. Lett. (in press).

8. A.J. Williamson, C. Bostedt, T. van Buuren, T.M. Willey, L.J. Terminello, G. Galli, and L. Pizzagalli, Nano Lett. **4**, 1041 (2004).

9. C. Bostedt, T. van Buuren, T.M. Willey, N. Franco, T. Möller, and L.J. Terminello, J. Electron Spectrosc. Relat. Phenom. **126**, 117 (2002).

10. S. Hayashi, M. Ito, and H. Kanamori, Solid State Commun. **44**, 75 (1982); S. Hayashi and K. Yamamoto, Superlattices & Microstructures **2**, 581 (1986).

11. M. Fujii, S. Hayashi, and K. Yamamoto, Appl. Phys. Lett. **57**, 2692 (1990).

12. J.M. Carpenter and D.L. Price, Phys. Rev. Lett. **54**, 441 (1985).

13. Shang-Fen Ren and Wei cheng, Phys. Rev. B **66**, 205328 (2002); Wei Cheng, Shang-Fen Ren, and Peter Y. Yu, Phys. Rev. B **68**, 193309 (2003).

14. T. Deegan and G. Hughes, Appl. Surf. Sci. **123-124**, 66 (1998); I.-M. Lee and C.G. Takoudis, J. Vac. Sci. Technol. A **15**, 3154 (1997).

15. H.I. Liu, D.K. Biegelsen, F.A. Ponce, N.M. Johnson, and R.F.W. Pease, Appl. Phys. Lett. **64**, 1383 (1994).

16. Krishna G. Nath, I. Shimoyama, T. Sekiguchi, and Y. Baba, Appl. Surf. Sci. **234**, 234 (2004); K.C. Scheer, R.A. Rao, R. Muralidhar, S. Bagchi, J. Conner, L. Lozano, C. Perez, M. Sadd, and B.E. White Jr., J. Appl. Phys. **93**, 5637 (2003).